Differential Roles for Endothelial ICAM-1, ICAM-2, and VCAM-1 in Shear-Resistant T Cell Arrest, Polarization, and Directed Crawling on Blood–Brain Barrier Endothelium

Oliver Steiner,* Caroline Coisne,* Roméo Cecchelli,† Rémy Boscacci,* Urban Deutsch,* Britta Engelhardt,* and Ruth Lyck*

Endothelial ICAM-1 and ICAM-2 were shown to be essential for T cell diapedesis across the blood–brain barrier (BBB) in vitro under static conditions. Crawling of T cells prior to diapedesis was only recently revealed to occur preferentially against the direction of blood flow on the endothelial surface of inflamed brain microvessels in vivo. Using live cell-imaging techniques, we prove that Th1 memory/effector T cells predominantly crawl against the direction of flow on the surface of BBB endothelium in vitro. Analysis of T cell interaction with wild-type, ICAM-1–deficient, ICAM-2–deficient, or ICAM-1 and ICAM-2 double-deficient primary mouse brain microvascular endothelial cells under physiological flow conditions allowed us to dissect the individual contributions of endothelial ICAM-1, ICAM-2, and VCAM-1 to shear-resistant T cell arrest, polarization, and crawling. Although T cell arrest was mediated by endothelial ICAM-1 and VCAM-1, T cell polarization and crawling were mediated by endothelial ICAM-1 and ICAM-2 but not by endothelial VCAM-1. Therefore, our data delineate a sequential involvement of endothelial ICAM-1 and VCAM-1 in mediating shear-resistant T cell arrest, followed by endothelial ICAM-1 and ICAM-2 in mediating T cell crawling to sites permissive for diapedesis across BBB endothelium. ***The Journal of Immunology*****, 2010, 185: 4846–4855.**

Interaction of T cells with the vascular endothelium is a critical step during T cell extravasation from blood into tissue in immunosurveillance and inflammation. Extravasation of T cells has been characterized as a multistep process involving T cell rolling along the vascular surface, T cell arrest and crawling on the endothelium and, finally, diapedesis of T cells (1). During interaction with the endothelium, T cells have to resist detachment by the shear forces they are exposed to within the bloodstream. Interestingly, recent studies documented that crawling of T cells, as well as of neutrophils, is perpendicular or even against the direction of blood flow in vivo (2, 3). Thus, crawling of T cells on the luminal surface of the vasculature requires a spatiotemporal regulation of the adhesion strength between the T cell and the endothelium. It was shown that the α4-integrins α4β1 and α4β7 and the β2-integrin LFA-1 control shear-resistant interactions of T cells with the endothelium (4). In fact, the polarized distribution of intermediate-affinity and high-affinity forms of LFA-1 along the T cell axis has been observed during postarrest T lymphocyte crawling on the endothelial luminal surface or on immobilized ICAM-1 (5, 6).

T cell interactions with the blood–brain barrier (BBB) endothelium may be unique because of the high specialization of these endothelial cells in building a tight barrier to maintain CNS homeostasis (7). BBB endothelial cells inhibit transcellular passage of molecules as a result of an extremely low pinocytotic activity and restrict the paracellular diffusion of hydrophilic molecules by an elaborate network of complex and P-face–associated tight junctions between endothelial cells (8). When brain endothelial cells are isolated and cultured in vitro, they rapidly lose many of their BBB characteristics, including formation of proper tight junctions and a permeability barrier, indicating that integrity of the BBB strictly depends on signals provided by the CNS microenvironment. This is confirmed by observations made with brain-derived endothelioma cells, which maintain some BBB characteristics but lose expression of a number of BBB-specific junctional molecules and, therefore, their barrier characteristics (9). Barrier characteristics of brain endothelium extend to the regulation of lymphocyte trafficking into the CNS. During physiological conditions, lymphocyte migration across the BBB is very low and restricted to highly activated lymphocytes (10–12). However, during inflammatory diseases of the CNS, such as multiple sclerosis (MS), circulating immunocompetent cells readily gain access to the CNS, where they induce inflammation, edema formation, and BBB breakdown, which together establish the clinical picture of the disease (2, 11).

Using brain endothelial cells under static conditions, we showed that endothelial VCAM-1 contributes to T cell adhesion, whereas endothelial ICAM-1 and ICAM-2 are important for T cell adhesion and diapedesis (13–16). However, the selective roles of endothelial VCAM-1, ICAM-1, and ICAM-2 in mediating shear-resistant

*Theodor Kocher Institute, University of Bern, Bern, Switzerland; and †Université Lille-Nord de France, Lens, France

Received for publication November 19, 2009. Accepted for publication August 5, 2010.

This work was supported by the European Stroke Network (Grants EU FP7 No. 201024 and No. 202213 to R.C. and B.E.) and by grants from the Swiss Multiple Sclerosis Society, the Novartis Foundation for Biomedical Research, and the SwissLife Foundation (to R.L.). O.S. received a one-year fellowship from the French Multiple Sclerosis Research Society, Fondation pour l'Aide à la Recherche sur la Sclérose En Plaques.

Address correspondence and reprint requests to Dr. Britta Engelhardt and Dr. Ruth Lyck, Theodor Kocher Institute, University of Bern, Freiestrasse 1, 3012 Bern, Switzerland. E-mail addresses: bengel@tki.unibe.ch and ruth.lyck@tki.unibe.ch

The online version of this article contains supplemental material.

Abbreviations used in this paper: BBB, blood–brain barrier; D_{acc}, accumulated total distance of T cell movement; D_x, straight *x*-axis distance covered by the T cell; EAE, experimental autoimmune encephalomyelitis; FOV, field of view; I1-KO, ICAM-1 deficient; I1/I2-KO, ICAM-1 and ICAM-2 deficient; I2-KO, ICAM-2 deficient; IF, immunofluorescence; mICAM-1, mouse ICAM-1/Fc; mICAM-2, mouse ICAM-2/Fc; MS, multiple sclerosis; mVCAM-1, mouse VCAM-1/Fc; $P_{e\ 3kDa}$, permeability coefficient for 3-kDa dextran; $P_{e\ 10kDa}$, permeability coefficient for 10-kDa dextran; PLP, proteolipid protein; pMBMEC, primary mouse brain microvascular endothelial cell; wt, wild-type; xFMI, forward migration index toward *x*-axis.

T cell arrest, versus T cell polarization and T cell crawling on the surface of brain endothelium, under physiological flow conditions have not been investigated. In this study, we specifically focused on dissecting the individual contributions of these endothelial cell adhesion molecules in the different steps of T cell extravasation across the BBB in vitro. Using wild-type (wt), ICAM-1–deficient (I1-KO), ICAM-2–deficient (I2-KO), or ICAM-1 and ICAM-2 deficient (I1/I2-KO) primary mouse brain microvascular endothelial cells (pMBMECs) freshly isolated prior to each experiment from the respective mice, we analyzed arrest, polarization, crawling velocity, crawling direction, and diapedesis of encephalitogenic Th1 memory/effector cells across the highly specialized BBB endothelium under physiological flow conditions. The specific function of VCAM-1 for T cell arrest was substantiated by Ab masking of endothelial VCAM-1 on pMBMECs. Recombinant mouse ICAM-1, ICAM-2, and VCAM-1 were used to analyze the individual roles of each cell adhesion molecule in supporting arrest, polarization, and crawling against the direction of shear. In summary, we demonstrate that endothelial ICAM-1 and VCAM-1, but not ICAM-2, mediate shear-resistant T cell arrest on BBB endothelium. Subsequently, endothelial ICAM-1 or ICAM-2, but not VCAM-1, is sufficient to mediate T cell polarization and crawling on the surface of the BBB, because both events are completely abrogated in the absence of ICAM-1 and ICAM-2. Endothelial ICAM-1 but not ICAM-2 enables T cells to crawl against the direction of flow on the BBB endothelium in vitro.

Materials and Methods

pMBMECs

pMBMECs were isolated from gender-matched 4–6-wk-old C57BL/6 mice (Harlan Laboratories, Horst, The Netherlands), cultured as described, and used nonpassaged on day 5 or 6 after isolation (9, 17). Stimulated pMBMECs were cultured for 16–18 h in the presence of TNF-α (25 ng/ml). All experiments were performed in migration assay medium (DMEM, 5% calf serum, 25 mM HEPES) at 37°C. I1-KO and I2-KO mice (18, 19) were backcrossed onto C57BL/6 mice for at least eight generations. I1/I2-KO C57BL/6 mice were obtained by breeding I1-KO mice with I2-KO C57BL/6 mice. All animal procedures were performed in accordance with the Swiss legislation on the protection of animals and were approved by the veterinary office of the Kanton of Bern.

T cells

The proteolipid protein (PLP)-specific $CD4^+$ Th1 effector/memory T cell line SJL.PLP7 raised against the PLP peptide $aa_{139–153}$ was described in detail (13). T cells were used 3 d after the third or fourth restimulation with their specific PLP Ag.

Permeability assay

Permeability assays were performed in triplicates for one value within each assay, as published (17), with minor adaptations: BBB endothelial cells were grown on Matrigel-coated filter inserts (0.4 μm pore size, 6.5 mm diameter; Transwell, VITARIS, Baar, Switzerland). Alexa Fluor 680-dextran (3 or 10 kDa, 10 μg/ml; LuBioScience, Luzerne, Switzerland) was used as permeability tracer. Diffused dextran was quantified using the Odyssey Imaging System (LI-COR, Bad Homburg, Germany).

T cell adhesion and diapedesis under static conditions

T cell adhesion and diapedesis assays were performed, as described previously (16, 20), in triplicates for one value in each experiment.

Coating of cell-culture dishes with recombinant cell-adhesion molecules

For live cell imaging of T cell interaction with recombinant purified cell-adhesion molecules, mouse ICAM-1/Fc (mICAM-1), ICAM-2/Fc (mICAM-2), and VCAM-1/Fc (mVCAM-1) (R&D Systems, Abingdon, U.K.) were bound to culture dishes whose surfaces were coated (1 h at 37°C, 20 μg/ml in PBS [pH 9]) with protein A (BioVision, Axxora Europe, Lausen, Switzerland). Protein A was overlaid with mICAM-1 or mVCAM-1 (10 μg/ml in PBS [pH 7.4]) or mICAM-2 (6.6 μg/ml in PBS, [pH 7.4] to keep equal molarity with ICAM-1) for 2 h at 37°C. Surfaces were blocked with 1.5% BSA in PBS (pH 7.4) for 30 min before use. Lack of unspecific T cell interactions with the substratum was tested in control experiments using protein A surfaces blocked with BSA or protein A overlaid with the rat IgG2a Ab 9B5 directed against human CD44.

Live cell imaging under flow conditions

For live cell imaging, a parallel flow chamber (21) connected to an automated syringe pump (Harvard Apparatus, Holliston, MA) was mounted on TNF-α–stimulated pMBMECs or on immobilized mICAM-1, mICAM-2, or mVCAM-1 and placed on the heating stage of an inverted microscope (imaging of T cell interaction with pMBMECs: Axiovert 200; imaging of T cell interaction with immobilized mICAM-1, mICAM-2 or mVCAM-1: AxioObserver Z1; both microscopes from Carl Zeiss, Feldbach, Switzerland). Shear stress (dyn/cm^2) was calculated according to the equation: $\tau = 3\mu Q/2a^2b$, where τ is wall shear stress, μ is coefficient of viscosity, Q is volumetric flow rate, a is half channel height, and b is channel width (22). T cells (5×10^5/ml) were allowed to accumulate for 4 min at low shear stress (0.25 dyn/cm^2). Then, dynamic T cell interactions with pMBMECs or immobilized mICAM-1, mICAM-2, or mVCAM-1 were recorded under physiological shear stress (1.5 dyn/cm^2) at ×100 magnification (pMBMECs: objective A-Plan ×10/0.25; mICAM-1, mICAM-2, or mVCAM-1: objective EC Plan Neofluar ×10/0.3) using a monochrome CCD camera (pMBMECs: Cohu, Poway, CA, connected to a digital video recording system; mICAM-1, mICAM-2, or mVCAM-1: AxioCam MRm Rev, Carl Zeiss). Time-lapse videos were created from one frame every 30 s (pMBMECs: iMovie, Apple, Cupertino, CA; mICAM-1, mICAM-2, or mVCAM-1: AxioVision, Carl Zeiss).

Statistical analyses

Unless noted otherwise, data are presented as mean ± SEM, and differences between two groups were analyzed by the unpaired Student t test. For three or more groups, one-way ANOVA was performed, followed by the Tukey multiple comparison test. A p value <0.05 was considered significant. Statistical analysis was done using GraphPad Prism 5 software (GraphPad, San Diego, CA).

Results

Absence of endothelial ICAM-1 and ICAM-2 has no influence on barrier characteristics of pMBMECs in vitro

In this study, we aimed to elucidate the selective roles of endothelial ICAM-1 versus ICAM-2 and VCAM-1 for T cell arrest and crawling along the luminal surface of and their diapedesis across the highly specialized BBB endothelium. Considering the unique barrier characteristics of brain endothelium, we specifically established an in vitro BBB model with pMBMECs, as described previously (17). To this end, pMBMECs were isolated from wt, I1-KO, I2-KO, and I1/I2-KO C57BL/6 mice. All types of pMBMECs formed confluent endothelial monolayers without any apparent morphological differences. Endothelial purity was confirmed for all four types of pMBMECs by uniformly positive immunofluorescence (IF) staining for the endothelial marker protein von Willebrand factor (Supplemental Fig. 1*A*). Because the molecular architecture of the BBB endothelial intercellular junctions is highly specialized, we carefully examined the molecular composition of the endothelial junctions of wt, I1-KO, I2-KO, and I1/I2-KO pMBMECs by IF analysis. We detected expression and proper junctional localization of the endothelial adherens junction molecule vascular endothelial-cadherin and of the tight junction proteins claudin-5, claudin-3, occludin, and junctional adhesion molecule-A. Additionally, platelet endothelial cell adhesion molecule-1 and the intracellular junction-associated scaffolding proteins zonula occludens-1 and -2 were found to be localized in the endothelial cell contacts, independent of the presence or absence of ICAM-1 and ICAM-2 (Supplemental Fig. 1*A*, 1*B*). Stimulation of wt pMBMECs with TNF-α induced upregulation of ICAM-1 and VCAM-1 on the endothelial cell surface, whereas cell-surface levels of ICAM-2 remained unchanged. We found ICAM-1, ICAM-2, and VCAM-1

localized to the endothelial surface, with minor or no staining of the intercellular junctions (Supplemental Fig. 1*C*). ICAM-1 or ICAM-2 cell-surface expression was missing on the respective ICAM-deficient pMBMECs under control and stimulatory conditions (data not shown). By careful visual comparison of equally stained and recorded IF images, we found comparable expression levels of ICAM-1 or ICAM-2 under control and inflammatory conditions on those pMBMECs expressing the respective molecules (Supplemental Fig. 1*D*).

To demonstrate overall tightness of monolayers formed by pMBMECs, we performed permeability assays with 3- and 10-kDa dextran as low molecular paracellular tracers. First, we compared pMBMECs with bEnd5, which is a brain-derived endothelioma cell line that has lost BBB-specific complexity of tight junction organization (9). For pMBMECs we determined a mean permeability coefficient for 3-kDa dextran ($P_{e\ 3kDa}$) of $0.12 \pm 0.01 \times 10^{-3}$ cm/min and for 10-kDa dextran ($P_{e\ 10kDa}$) of $0.06 \pm 0.01 \times 10^{-3}$ cm/min. For bEnd5, $P_{e\ 3kDa}$ was $2.20 \pm 0.29 \times 10^{-3}$ cm/min and $P_{e\ 10kDa}$ was $0.91 \pm 0.16 \times 10^{-3}$ cm/min. Therefore, the permeability coefficients for 3- and 10-kDa dextran for pMBMECs were 18-fold ($P_{e\ 3kDa}$) or 15-fold ($P_{e\ 10kDa}$) lower than for bEnd5, demonstrating the strikingly reduced paracellular permeability of pMBMECs compared with bEnd5 (Supplemental Fig. 2). Thus, pMBMECs form tight monolayers in vitro.

Next, we tested whether the absence of ICAM-1 and/or ICAM-2 influences pMBMEC barrier integrity. To this end, we compared the paracellular permeability of wt pMBMECs with the respective paracellular permeabilities of I1-KO, I2-KO, and I1/I2-KO pMBMECs. The $P_{e\ 3kDa}$ values for I1-KO, I2-KO, and I1/I2-KO pMBMECs showed no significant differences compared with wt pMBMECs (I1-KO $P_{e\ 3kDa}$, $0.10 \pm 0.02 \times 10^{-3}$ cm/min; I2-KO $P_{e\ 3kDa}$, $0.15 \pm 0.03 \times 10^{-3}$ cm/min; and I1/I2-KO $P_{e\ 3kDa}$, $0.15 \pm 0.03 \times 10^{-3}$ cm/min) (Fig. 1*A*). Likewise, permeability coefficient values obtained for 10-kDa dextran confirmed the comparable tightness of all four types of pMBMECs (I1-KO $P_{e\ 10kDa}$, $0.05 \pm 0.01 \times 10^{-3}$ cm/min; I2-KO $P_{e\ 10kDa}$, $0.08 \pm 0.01 \times 10^{-3}$ cm/min; and I1/I2-KO $P_{e\ 10kDa}$, $0.08 \pm 0.01 \times 10^{-3}$ cm/min) (Fig. 1*B*). In summary, pMBMECs formed a tight BBB in vitro, independent of the presence or absence of ICAM-1 or ICAM-2.

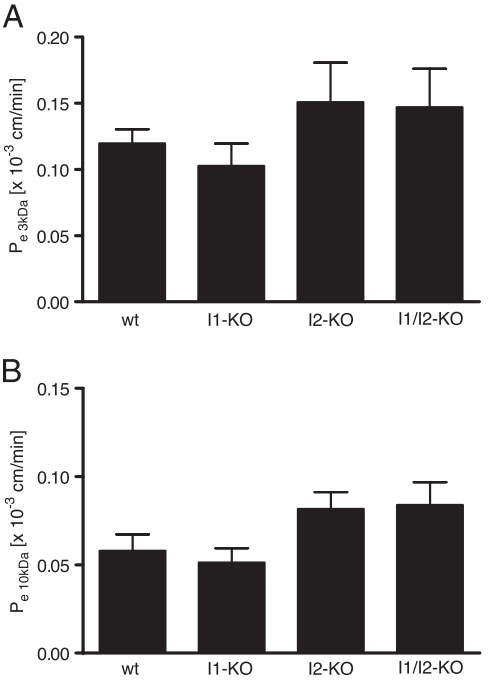

FIGURE 1. Unchanged permeabilities of wt, I1-KO, I2-KO, and I1/I2-KO BBB endothelium. $P_{e\ 3kDa}$ (*A*) and $P_{e\ 10kDa}$ (*B*) for wt, I1-KO, I2-KO, and I1/I2-KO pMBMECs. Permeability coefficients for endothelial monolayers were calculated from diffused Alexa Fluor 680-dextran (four time points of 10 min each), as published (36). Bars represent mean ± SEM of at least three independent experiments. One-way ANOVA, followed by the Tukey multiple-comparison test, confirmed the absence of significant differences (all p values >0.05).

Endothelial ICAM-1 is essential for T cell adhesion to and diapedesis across the BBB under static conditions

To ensure the validity of our previous findings on the roles of endothelial ICAM-1 and ICAM-2 in Th1 cell adhesion to and diapedesis across immortalized brain endothelioma cells, which do not form a tight permeability barrier in vitro, we reassessed the involvement of endothelial ICAM-1 and ICAM-2 in T cell interaction with the in vitro BBB (15, 16, 18). To this end, we investigated T cell adhesion and diapedesis across pMBMECs under static conditions. First, we compared T cell interaction with unstimulated and TNF-α–stimulated wt pMBMECs. As expected, stimulation of pMBMECs with TNF-α induced a strong upregulation of T cell adhesion (2.1-fold increase) and T cell diapedesis (2.5-fold increase) compared with unstimulated pMBMECs (Supplemental Fig. 3).

Next, we compared T cell adhesion to I1-KO, I2-KO, and I1/I2-KO pMBMECs with T cell adhesion to wt pMBMECs (100%) under unstimulated and TNF-α–stimulated conditions (Fig. 2*A*). Under both conditions, T cell adhesion to I1-KO pMBMECs was significantly reduced (unstimulated, 37.5 ± 4.8%; TNF-α stimulated, 79.4 ± 6.5%) compared with wt pMBMECs. In contrast, T cell adhesion to I2-KO pMBMECs remained unchanged (unstimulated, 92.7 ± 12.5%; TNF-α stimulated, 98.7 ± 1.0%). However, a greater reduction in T cell adhesion to I1/I2-KO pMBMECs (unstimulated, 15.7 ± 3.1%; TNF-α stimulated, 42.1 ± 2.6%) demonstrated an additional role of endothelial ICAM-2 in T cell adhesion to brain endothelium, which was only detectable in the absence of endothelial ICAM-1 (Fig. 2*A*).

Comparing T cell diapedesis across I1-KO, I2-KO, and I1/I2-KO pMBMECs with T cell diapedesis across wt pMBMECs (100%) under unstimulated and TNF-α stimulated conditions (Fig. 2*B*), we found results similar to T cell adhesion. T cell diapedesis across I1-KO or I1/I2-KO pMBMECs was strongly reduced (I1-KO: unstimulated, 35.2 ± 8.9%, TNF-α stimulated, 51.3 ± 3.8%; I1/I2-KO: unstimulated, 43.6 ± 4.4%, TNF-α stimulated 47.3 ± 5.2%), but diapedesis of T cells across I2-KO pMBMECs remained unchanged (unstimulated I2-KO: 91.7 ± 11.9%, TNF-α–stimulated I2-KO: 114.2 ± 13.6%). Under these static conditions, an additional contribution of ICAM-2 to T cell diapedesis in the absence of ICAM-1 was not detectable, because the values obtained for T cell diapedesis across I1/I2-KO pMBMECs were similar to the values obtained for I1-KO pMBMECs.

Taken together, endothelial ICAM-1 fulfils a major function in T cell adhesion to and in T cell diapedesis across the BBB under static conditions. In the presence of endothelial ICAM-1, endothelial ICAM-2 is only of minor relevance for T cell interaction with pMBMECs. However, in the absence of endothelial ICAM-1, ICAM-2 was found to contribute to T cell adhesion to the BBB in vitro.

Endothelial ICAM-1 and VCAM-1, but not ICAM-2, mediate T cell arrest on the BBB under flow

Intermediate- and high-affinity forms of LFA-1 were described to control T cell dynamic interaction with the endothelium or on purified ICAM-1 under physiological flow (5, 6, 23). The experiments described above do not allow dissection of the role of

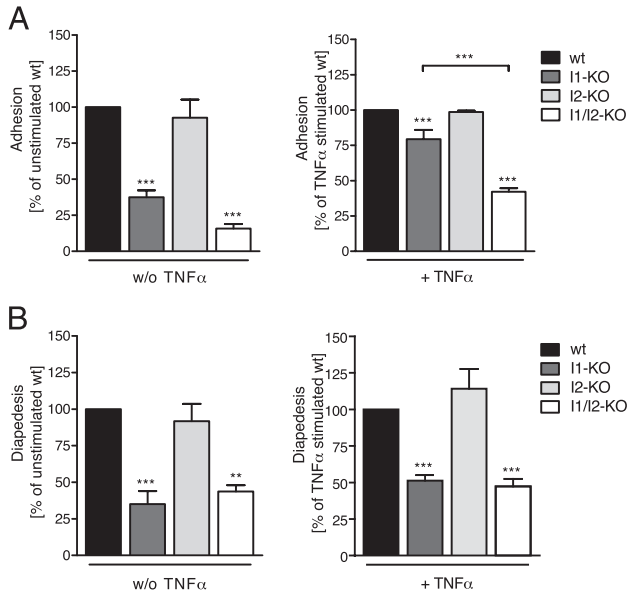

FIGURE 2. Essential contribution of endothelial ICAM-1 to T cell adhesion and diapedesis under static conditions. T cell adhesion to (*A*) and transmigration across (*B*) confluent wt, I1-KO, I2-KO, and I1/I2-KO pMBMECs. Because it was not possible to simultaneously isolate all four types of pMBMECs, we included wt pMBMECs in each experiment and set the values obtained for unstimulated (w/o TNF-α) or TNF-α–stimulated (+TNF-α) wt pMBMECs to 100%. One representative experiment each for T cell adhesion and T cell diapedesis and showing raw values are presented in Supplemental Fig. 2. *A*, Numbers of T cells adherent to wt, I1-KO, I2-KO, and I1/I2-KO pMBMECs were counted per FOV (600 × 600 μm) at ×200 magnification and expressed as the percentage of adherent T cells on wt pMBMECs. Data are mean ± SEM of seven independent experiments. *B*, T cell diapedesis across wt, I1-KO, I2-KO, and I1/I2-KO pMBMECs measured in a static two-chamber–based experimental setup (6 h migration time). Within one experiment, each value for diapedesed T cells was calculated as percentage of input. For comparison among different experiments, the value obtained for wt pMBMECs was set to 100%. Bars represent mean ± SEM of 12 independent experiments. $^{**}p < 0.01$; $^{***}p < 0.001$, versus wt; one-way ANOVA, followed by the Tukey multiple-comparison test.

endothelial ICAM-1 and ICAM-2 in shear-resistant T cell arrest and crawling on the BBB prior to their diapedesis across the BBB. Therefore, we investigated the roles of endothelial ICAM-1 and ICAM-2 in T cell interaction with the BBB in vitro by performing live cell imaging in a flow chamber experimental setup. We specifically focused on inflammatory conditions of the BBB with regard to the relevance for T cell trafficking across the BBB in chronic inflammatory diseases, such as MS. T cells were perfused over a monolayer of pMBMECs at low shear stress (0.25 dyn/cm^2) to allow for their accumulation. Subsequently, shear stress was increased to physiological strength (1.5 dyn/cm^2), and T cell interaction with pMBMECs was recorded under constant flow over 30 min. To determine the number of T cells that arrested in a shear-resistant manner to the pMBMEC monolayer during the accumulation phase, we analyzed one image acquired after the first 30 s of enhanced shear stress and counted the numbers of arrested T cells per field of view (FOV). These T cells, which initially adhered under low shear stress and resisted immediate flow enhancement, were named arrested T cells.

We counted 88 ± 7 arrested T cells per FOV on wt pMBMECs. A significant contribution of endothelial ICAM-1 to T cell arrest on the BBB was shown by a reduction in arrested T cells by 48 and 50% on I1-KO (46 ± 4 T cells/FOV) and I1/I2-KO pMBMECs (44 ± 3 T cells/FOV), respectively, compared with wt pMBMECs (Fig. 3*A*). Lack of ICAM-2 on I2-KO pMBMECs did not result in significantly reduced numbers of arrested T cells compared with wt pMBMECs (Fig. 3*A*). In contrast to static T cell-adhesion experiments, we counted equal numbers of T cells firmly arrested on I1-KO and I1/I2-KO pMBMECs, demonstrating that endothelial ICAM-2 does not significantly contribute to initial shear-resistant T cell arrest on pMBMECs.

To investigate the role of endothelial VCAM-1 in initial shear-resistant T cell arrest on the inflamed BBB, we masked VCAM-1 on TNF-α–stimulated wt, I1-KO, I2-KO, and I1/I2-KO pMBMECs with Ab prior to T cell perfusion. Although initial arrest of T cells on wt pMBMECs was reduced only marginally and nonsignificantly, a complete inhibition of T cell arrest was observed after blocking VCAM-1 on I1-KO and I1/I2-KO pMBMECs (Fig. 3*B*). Taken together, these observations demonstrate that endothelial ICAM-1 and VCAM-1, but not ICAM-2, mediated shear-resistant T cell arrest on the inflamed BBB in vitro.

To confirm the individual contributions of ICAM-1 and VCAM-1 versus ICAM-2 in mediating shear-resistant T cell arrest in a cell-independent context, we investigated the individual abilities of immobilized recombinant murine ICAM-1, ICAM-2, and VCAM-1 to support shear-resistant T cell arrest. On immobilized ICAM-1 or VCAM-1, 122 ± 5 and 104 ± 4 T cells arrested per FOV, respectively, supporting the notion that both cell-adhesion molecules efficiently support T cell arrest under flow (Fig. 3*C*). In contrast, immobilized ICAM-2 was significantly less efficient in supporting T cell arrest, with 60 ± 4 T cells counted per FOV (Fig. 3*C*).

Therefore, our data demonstrate a dominant role for endothelial ICAM-1 and VCAM-1 in mediating shear-resistant T cell arrest. The moderate intrinsic ability of ICAM-2 to support T cell arrest under flow is fully masked when ICAM-2 is displayed in its physiological context on the pMBMEC membrane in the presence of ICAM-1 and VCAM-1.

Endothelial ICAM-1 and ICAM-2, but not VCAM-1, mediate T cell polarization and crawling on the BBB under flow

After their shear-resistant arrest on the endothelial surface, T cells rapidly acquired a polarized cell shape, with a characteristic broad lamellipodium at the cell front and a typical elongated and projected uropod at the trailing edge (Fig. 4*A*), and started crawling. During the 30-min observation period, T cells continuously crawled on the surface of the pMBMECs or transiently crawled on the surface of the brain endothelial cells, followed by diapedesis through the monolayer (Supplemental Video 1). T cells that failed to diapedese across the brain endothelium within the 30 min of recording time covered strikingly longer distances on the brain endothelial surface than T cells that underwent diapedesis.

To analyze the individual contributions of endothelial ICAM-1 and endothelial ICAM-2 to T cell polarization, crawling, and diapedesis, we performed a visual frame-by-frame offline analysis of the dynamic behavior of T cells arrested on wt, I1-KO, I2-KO, and I1/I2-KO pMBMECs and assigned each arrested T cell to one of the following four groups: T cells that crawled and diapedesed, T cells that continuously crawled without diapedesis, T cells that stayed stationary, and T cells that detached and failed to maintain firm adhesion under enhanced shear. The numbers of initially arrested T cells on the respective pMBMECs under low shear stress were set to 100%, and each category was expressed as the fraction of arrested T cells. On wt pMBMECs, the majority (52.2 ± 8.9%) of T cells underwent diapedesis after a crawling phase, and 42.1 ± 9.2% of T cells crawled continuously during the observation period. Only a minor fraction of T cells (4.6 ± 1.3%) remained stationary on wt pMBMECs, and a very small number (1.2 ± 0.1%) failed to maintain adhesion and detached from pMBMECs (Fig. 4*B*).

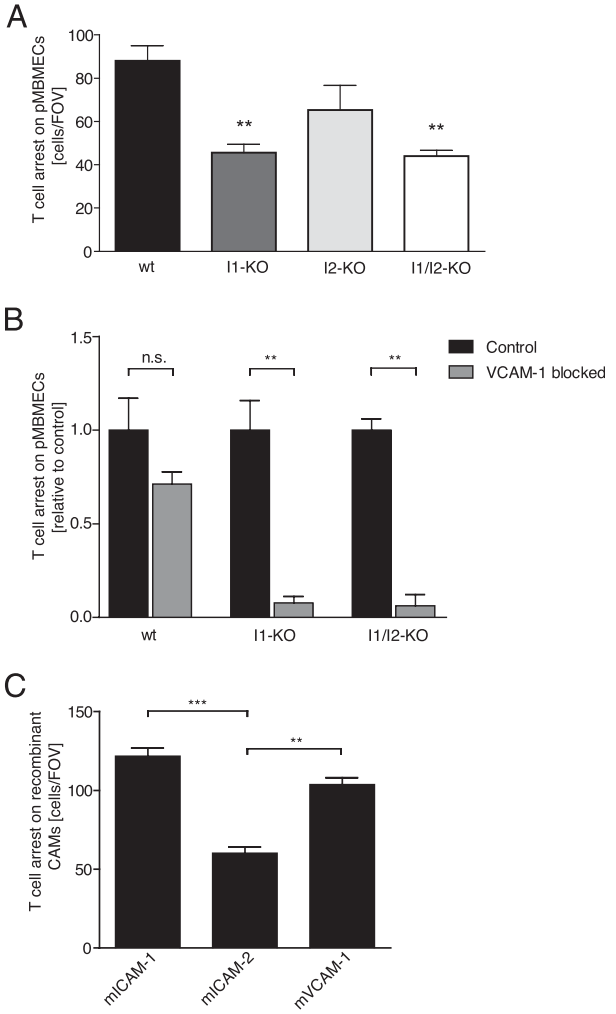

FIGURE 3. Essential roles for endothelial ICAM-1 and VCAM-1 in T cell arrest on pMBMECs under flow. T cells that arrested on the endothelium during the accumulation phase and resisted immediate detachment by enhanced shear stress were counted by evaluation of the first frame after flow enhancement to 1.5 dyn/cm^2. *A*, Numbers of arrested T cells per FOV (963 × 642 μm) on TNF-α–stimulated wt, I1-KO, I2-KO, and I1/I2-KO pMBMECs. *B*, wt, I1-KO, or I1/I2-KO pMBMECs were incubated with blocking monoclonal anti–VCAM-1 Ab (MK2.7; 20 μg/ml) for 15 min prior to the flow experiment. *C*, Numbers of arrested T cells per FOV (865 × 650 μm) on immobilized recombinant mICAM-1, mICAM-2, or mVCAM-1. Data are mean ± SEM from three independent experiments for each group. $**p < 0.01$; $***p < 0.001$, compared with wt; one-way ANOVA, followed by the Tukey multiple-comparison test.

In the absence of endothelial ICAM-1 on I1-KO pMBMECs, a significantly reduced percentage of T cells (28.2 ± 5.6%) crawled and diapedesed compared with wt pMBMECs. This was accompanied by an increase in the percentage of T cells that remained stationary (19.1 ± 1.0%) or that detached from I1-KO pMBMECs (6.0 ± 3.1%). Interestingly, the fraction of T cells that crawled continuously on I1-KO pMBMECs remained unchanged (46.7 ± 2.7%) compared with wt pMBMECs (Fig. 4*B*). Lack of endothelial ICAM-2 on I2-KO pMBMECs did not result in any significant changes in the dynamic behavior of T cells compared with wt pMBMECs.

However, dramatic changes in the dynamic T cell behavior on the endothelium were obvious in the absence of endothelial ICAM-1 and ICAM-2. In contrast to wt, I1-KO, or I2-KO pMBMECs, the T cells that arrested on I1/I2-KO pMBMECs failed to acquire polarized cell morphology and did not crawl on the endothelium

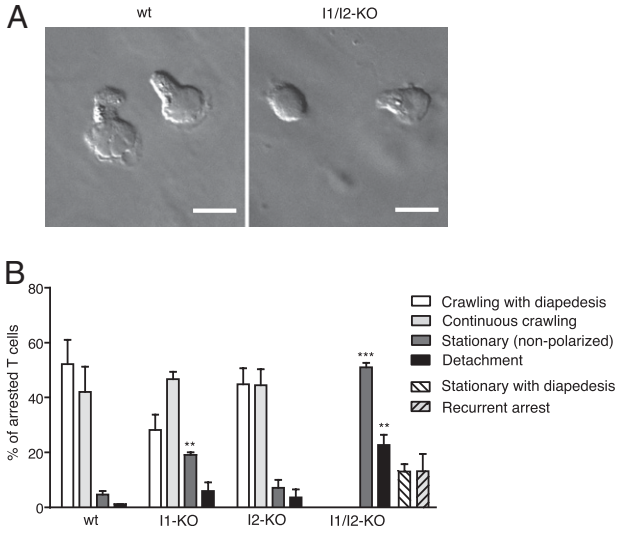

FIGURE 4. Individual roles of endothelial ICAM-1 and ICAM-2 in polarization, crawling, diapedesis, and resistance to detachment of T cells interacting with BBB endothelium under flow. *A*, Different morphologies of T cells on wt (*left panel*) or I1/I2-KO (*right panel*) brain endothelium. Differential interference contrast images were taken of T cells that were in contact with TNF-α–stimulated pMBMECs for 12 min under enhanced flow and subsequently fixed with 4% PFA. Original magnification ×400; scale bars, 10 μm. *B*, Characterization of dynamic T cell interactions with TNF-α–stimulated wt, I1-KO, I2-KO, or I1/I2-KO pMBMECs under flow conditions. Crawling with diapedesis represents T cells that polarized and crawled until they finally crossed the endothelial cell monolayer (identified by a characteristic change in brightness under phase-contrast illumination). Continuous crawling represents T cells that polarized and crawled at least two T cell diameters but did not diapedese across the endothelium. Stationary represents T cells that remained stationary (less than two T cell diameters of movement from their site of arrest). Detachment represents T cells that detached during the 30 min of recording under physiological shear stress. Two additional categories were defined based on observations of T cell behavior on I1/I2-KO pMBMECs: stationary with diapedesis represents T cells that remained stationary but finally crossed the endothelial cell monolayer, and recurrent arrest represents T cells that dislocated from the site of arrest in the absence of polarization and crawling. Data are mean ± SEM from three independent experiments for each group. $**p < 0.01$; $***p < 0.001$, compared with wt; one-way ANOVA, followed by the Tukey multiple-comparison test.

(Fig. 4*A*). Most of these T cells (51.0 ± 1.7%) remained stationary throughout the entire observation period (Fig. 4*B*, Supplemental Video 2). In addition, a significantly increased fraction of initially arrested T cells detached from I1/I2-KO pMBMECs (22.8 ± 3.6%), indicating a defect in shear-resistant T cell firm adhesion on pMBMECs lacking ICAM-1 and ICAM-2. Despite the lack of polarization and crawling, few T cells dislocated from their original site of arrest. This movement of T cells on I1/I2-KO pMBMECs was always along the direction of flow and resembled consecutive sequences of detachment and parallel reattachment to the endothelium. The particular T cell behavior on I1/I2-KO pMBMECs differed markedly from the effective crawling of highly polarized T cells observed on wt, I1-KO, or I2-KO pMBMECs; instead, it resembled a recurrent arrest behavior of T cells. Therefore, we assigned the T cell dislocation on I1/I2-KO pMBMECs (13.2 ± 6.3% of T cells) to a different category that we named "recurrent arrest" (Fig. 4*B*). Interestingly, a small fraction of T cells (13.1 ± 2.6%) that remained stationary were able to diapedese across I1/I2-KO pMBMECs at the site of their initial arrest. Taken together, our findings demonstrate that endothelial ICAM-1 and ICAM-2 are essential for polarization and crawling of T cells on the in-

flamed BBB under flow conditions. Lack of endothelial ICAM-1 and ICAM-2 results in a dramatically reduced T cell diapedesis across the BBB. Interestingly, however, a few diapedesis events still occurred, independent of endothelial ICAM-1 and ICAM-2.

To further delineate the contributions of ICAM-1, ICAM-2, and VCAM-1 to the support of T cell polarization and crawling, we analyzed T cell behavior on immobilized recombinant mouse ICAM-1, ICAM-2, and VCAM-1 after their initial arrest under shear for an observation period of 15 min (Fig. 5*A*, Supplemental Videos 3–5). On ICAM-1 and ICAM-2, 95.0 ± 1.3% and 89.0 ± 4.1%, respectively, of the arrested T cells polarized rapidly and started to crawl (Fig. 5*B*), whereas only a few T cells (2.8 ± 1.5 and 0%, respectively) remained stationary. These observations support the assertion that both molecules support T cell polarization and crawling equally well. A lower avidity of T cell interaction with ICAM-2, compared with ICAM-1, was demonstrated by the observation that only 2.2 ± 0.3% of T cells detached from ICAM-1 versus 11.1 ± 4.1% from ICAM-2 during the observation period.

Similar to ICAM-1 and ICAM-2, few T cells (4.3 ± 1.1%) remained stationary on immobilized VCAM-1. However, in striking contrast to T cell behavior on immobilized ICAM-1 and ICAM-2, T cells failed to completely polarize, flatten, and crawl on VCAM-1. Measuring the mean length of T cells interacting with ICAM-1 versus VCAM-1, from the leading edge to the trailing edge, further supported the notion that VCAM-1 fails to trigger complete T cell polarization; the mean length of T cells adhering to VCAM-1 was only 18.8 ± 0.35 μm compared with 23.1 ± 0.37 μm for those polarized and crawling on immobilized ICAM-1 (Supplemental Fig. 4*A*). Instead, most T cells interacting with immobilized VCAM-1 (65.0 ± 8.1%) repeatedly extended and retracted cell protrusions in all directions, resembling the recurrent arrest behavior of T cells observed on I1/I2-KO pMBMECs (Videos 2, 5). As a consequence, T cell interactions with VCAM-1 failed to establish stable adhesions over time, and a significantly greater percentage of T cells (30.8 ± 9.1%) detached from the VCAM-1–coated surface compared with ICAM-1– and ICAM-2–coated surfaces.

Taken together, our data clearly demonstrate that T cell polarization and crawling under physiological shear are supported by endothelial ICAM-1 and, in its absence, by endothelial ICAM-2. In contrast, although VCAM-1 supports repeated events of shear-resistant T cell arrest under physiological flow, it does not mediate T cell polarization and crawling; thus, it establishes less stable adhesive interactions with pMBMECs over time.

ICAM-1, but not ICAM-2, supports T cell crawling against the direction of flow on BBB endothelium

While observing T cell crawling on wt pMBMECs, it became obvious that the direction of crawling on the endothelium was not random. Rather, T cell crawling paths were predominantly oriented against the direction of flow (Fig. 6*A*), as recently observed for T cell interaction with meningeal blood vessels in vivo (2). To verify directed T cell crawling against the shear flow, we calculated a forward migration index toward the *x*-axis (xFMI), which was along the direction of flow in the FOV. On wt pMBMECs, the xFMI of T cells was found to be 0.13 ± 0.03, which differed significantly from 0, thereby proving T cell crawling against the direction of flow (Fig. 6*B*). Control experiments showed that, in the absence of shear flow, T cell crawling on wt pMBMECs occurred randomly in all directions (xFMI: 0.06 ± 0.03). Thus, flow conditions specifically induced T cell crawling on wt pMBMECs against the direction of shear forces.

To determine the individual contributions of endothelial ICAM-1 and ICAM-2 to directed T cell crawling on BBB endothelium, we compared xFMI values for T cell paths tracked on wt, I1-KO, I2-KO, and I1/I2-KO pMBMECs (Fig. 6*A*, 6*B*). For I1-KO pMBMECs, the xFMI was 0.0 ± 0.04, demonstrating that endothelial ICAM-1 is essential for the directed crawling of T cells against the flow on the inflamed BBB. This is further supported by the observation that I2-KO pMBMECs fully supported directed T cell crawling against the flow, comparable to wt pMBMECs, with the xFMI being 0.13 ± 0.04. T cells failed to polarize and crawl on I1/I2-KO pMBMECs. Rather, their behavior resembled recurrent arrest and detachment events. Nevertheless, to demon-

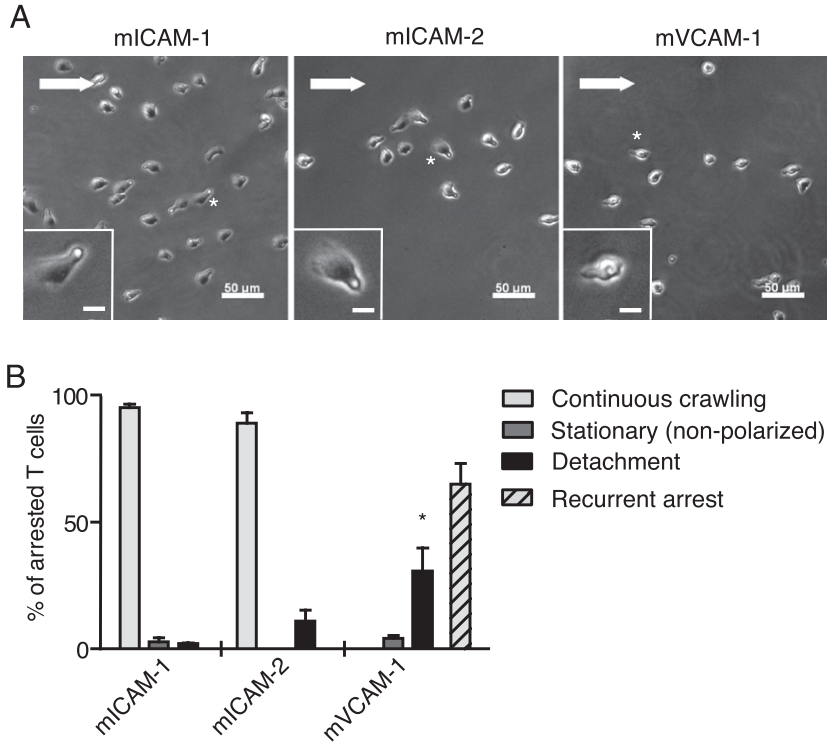

FIGURE 5. ICAM-1 and ICAM-2, but not VCAM-1, support T cell crawling under flow. Analysis of T cell interaction with immobilized recombinant mICAM-1, mICAM-2, or mVCAM-1 is shown. *A*, Representative images of crawling T cells on ICAM-1 or ICAM-2 or of recurrent arresting T cells on VCAM-1. Arrows indicate direction of shear flow (original magnification ×100). *Insets* show enlarged images of individual T cells marked with an asterisk (scale bar, 10 μm). *B*, Analysis of dynamic T cell interactions with mICAM-1, mICAM-2, or mVCAM-1. Continuous crawling represents T cells that polarized and crawled. Stationary represents T cells that remained stationary (less than two T cell diameters of movement from their site of arrest). Detachment represents T cells that detached during the 15 min of recording under physiological shear. Recurrent arrest represents T cells that dislocated from the site of arrest in the absence of polarization and crawling in a fashion resembling multiple detachment and reattachment cycles. Data are mean ± SEM from three independent experiments for each group. $*p < 0.05$, compared with wt; one-way ANOVA, followed by the Tukey multiple-comparison test.

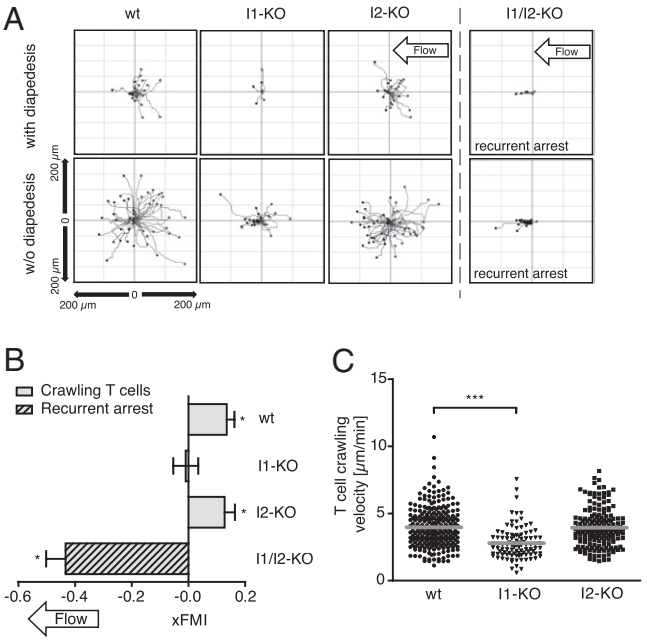

FIGURE 6. Differential roles of endothelial ICAM-1 and ICAM-2 in directed T cell crawling and crawling velocity on BBB endothelium under flow. Evaluations of T cell tracks on TNF-α–stimulated wt, I1-KO, I2-KO, and I1/I2-KO pMBMECs are shown. *A*, *x*/*y* diagrams of T cell tracks for one representative experiment in each group. T cell tracks were divided into two groups: T cells that underwent diapedesis (*upper panels*) and T cells that remained on the endothelium without diapedesis (*lower panels*). For each track, the site of arrest was set to the center point of the respective diagram. End points of tracks are indicated by dots. *B*, Directionality of T cell movements under shear flow expressed as xFMI ($xFMI = D_x/D_{acc}$ where D_x is straight *x*-axis distance covered by the T cell and D_{acc} is accumulated total distance of T cell movement). With relation to the FOV, the direction of flow was along the *x*-axis from plus to minus. Therefore, a positive xFMI value represents a directed crawling against the orientation of shear flow, whereas a negative xFMI value indicates movement along the shear forces. xFMI was calculated from T cell tracks of three independent videos per type of pMBMEC. Data are mean ± SEM. $*p < 0.05$, compared with random crawling (xFMI = 0); one-sample *t* test. *C*, Mean T cell crawling velocities (micrometers per minute) were calculated from three independent videos per type of pMBMEC (wt, I1-KO, I2-KO). Each data point represents the velocity of one T cell. $***p < 0.001$, one-way ANOVA, followed by the Tukey multiple-comparison test.

strate the failure of T cells to withstand shear forces in the absence of endothelial ICAM-1 and ICAM-2, we calculated the xFMI for these T cell interactions on I1/I2-KO pMBMECs. As expected, the xFMI for the direction of T cell movement on I1/I2-KO pMBMECs was negative (−0.43 ± 0.07).

Obviously, therefore, crawling of T cells on the surface of wt pMBMECs was mediated by endothelial ICAM-1 and ICAM-2. Although only endothelial ICAM-1 allowed for directed crawling against shear forces on BBB endothelium, perpendicular crawling of T cells on I1-KO pMBMECs was dependent on the presence of ICAM-2. To investigate whether T cell crawling velocities on I1-KO and I2-KO pMBMECs would also differ, we calculated mean velocities of T cells crawling on wt, I1-KO, and I2-KO pMBMECs. Because T cells failed to crawl on I1/I2-KO pMBMECs, we had to omit them from this analysis. Although the average T cell crawling velocity on wt pMBMECs was 4.0 ± 0.1 μm/min, we observed a significantly reduced T cell crawling velocity of 2.8 ± 0.1 μm/min in the absence of endothelial ICAM-1 on I1-KO pMBMECs (Fig. 6*C*). The velocity of T cell crawling on I2-KO pMBMECs remained unchanged compared with wt pMBMECs (Fig. 6*C*). Thus, T cell crawling velocity on BBB endothelium is defined by endothelial ICAM-1.

Purified immobilized ICAM-1 and ICAM-2, but not VCAM-1, support T cell crawling against the direction of flow

To analyze whether mechano-sensing for directed T cell crawling is a function of the endothelium or the T cell itself, we manually tracked T cells during their interaction with immobilized rICAM-1, rICAM-2, and rVCAM-1 (Fig. 7*A*). As the result of a different experimental set-up used for this particular analysis, shear flow was oriented opposite to the set-up described above for studying T cell interaction with pMBMECs; thus, a negative xFMI describes a predominant movement toward shear flow. As expected, in the absence of shear flow, postarrest T cell crawling tracks on immobilized ICAM-1 lacked any directionality (xFMI: 0.02 ± 0.04). When applying physiological flow, T cells crawled against the direction of flow on immobilized ICAM-1 and, surprisingly, in a similar manner on immobilized ICAM-2 (xFMI: −0.22 ± 0.03 and −0.26 ± 0.04, respectively) (Fig. 7*A*, 7*B*). In contrast, on immobilized VCAM-1, T cells exhibited recurrent arrest movements exclusively along the direction of flow (xFMI: 0.67 ± 0.02; Fig. 7*A*, 7*B*).

Because we determined that a significantly higher percentage of T cells detach from immobilized VCAM-1 compared with ICAM-1 (Fig. 5*B*), we speculated that the avidity of T cell interaction with immobilized ICAM-1 is higher than with immobilized VCAM-1. To further investigate this, we analyzed T cell detachment from immobilized ICAM-1 or VCAM-1 under enhanced shear forces. Stepwise enhancement of shear forces from 1.5–9.0 dyn/cm^2 minimally influenced the number of T cells adhering to immobilized ICAM-1, with 90 ± 10% of initially arrested T cells remaining in the FOV with shear forces of 9 dyn/cm^2 (Supplemental Fig. 4*B*). In contrast, on immobilized VCAM-1, T cells readily started to detach in parallel with the enhanced shear forces, with only 38 ± 5% of initially arrested T cells remaining attached at shear forces of 9.0 dyn/cm^2. Taken together, immobilized ICAM-1 and ICAM-2, but not VCAM-1, were able to support directional T cell crawling against the flow. The failure of VCAM-1 to support T cell polarization and crawling correlated with a reduced avidity of T cell interactions on immobilized VCAM-1 compared with ICAM-1.

To address whether crawling velocity is influenced by shear and differentially supported by ICAM-1 or ICAM-2, we calculated the mean velocities of T cells crawling on immobilized ICAM-1 and ICAM-2 (Fig. 7*C*). Interestingly, we found equal crawling velocities on rICAM-1, independent of the presence (8.5 ± 0.15 μm/min) or absence (7.9 ± 0.17 μm/min) of physiological shear. Unexpectedly, on immobilized ICAM-2, T cells crawled with an equal velocity (8.3 ± 0.22 μm/min) compared with on immobilized ICAM-1 (Fig. 7*C*).

In conclusion, the reduced T cell crawling velocity and lack of preferentially directed T cell crawling against the flow observed on I1-KO pMBMECs is not due to the intrinsic inability of ICAM-2 to support these features; rather, it seems to depend on the different accessibility of endothelial ICAM-2 in its physiological context on the pMBMEC surface membrane.

Discussion

In the current study, we dissected the individual contributions of brain endothelial ICAM-1, ICAM-2, and VCAM-1 in mediating shear-resistant T cell arrest, polarization, and directed crawling on BBB endothelium. We found that endothelial ICAM-1 and VCAM-1, but not ICAM-2, mediated shear-resistant T cell arrest on the BBB in vitro. Subsequent polarization and crawling of

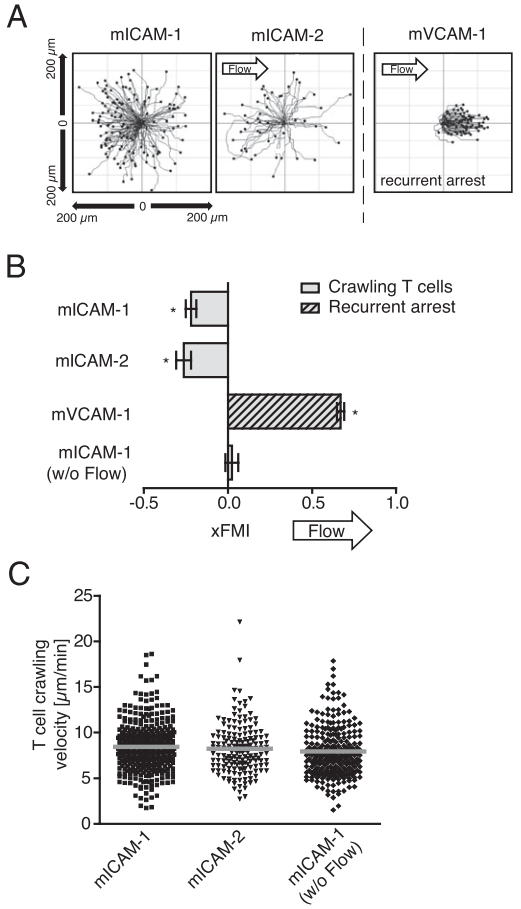

FIGURE 7. T cells crawl against the direction of flow on immobilized ICAM-1 and ICAM-2 but not on VCAM-1. Evaluation of T cell tracks on immobilized rICAM-1, rICAM-2, or rVCAM-1 under physiological shear. Note that because of a different experimental set-up, shear flow direction is opposite to the direction of flow shown in Fig. 6. *A*, *x*/*y* diagrams of T cell tracks are depicted for one representative experiment in each group. For each track, the site of arrest was set to the center point of the respective diagram. End points of tracks are indicated by dots. *B*, Directionality of T cell movements under shear flow is expressed as xFMI. In this particular experimental set-up, a negative xFMI demonstrates predominant movement against the direction of flow, and a positive xFMI describes a direction of movement along the shear flow. The xFMI was calculated from T cell tracks of three independent videos each. Data are mean ± SEM. $*p < 0.05$, compared with random crawling (xFMI = 0); one-sample *t* test. *C*, Mean T cell crawling velocities (micrometers per minute) were calculated from three independent movies each. Each data point represents the velocity of one T cell.

T cells to sites permissive for diapedesis across the BBB endothelium are mediated by endothelial ICAM-1 and ICAM-2; the absence of both completely abrogated T cell polarization and shear-resistant crawling on pMBMECs. Although immobilized purified ICAM-1 and ICAM-2 supported T cell crawling against the direction of flow, the presence of endothelial ICAM-1 on the cell surface of pMBMECs was strictly required for directed T cell crawling. We observed rare diapedesis events of noncrawling T cells across I1/I2-KO pMBMECs, suggesting that this particular step can occur independently of endothelial ICAM-1 and ICAM-2.

In previous studies using brain-derived endothelioma cell lines, we showed that both types of molecular interactions (α4-integrins with endothelial VCAM-1 and LFA-1 with endothelial ICAM-1 and ICAM-2) mediated the adhesion of encephalitogenic T cells to brain endothelium under static conditions in vitro. Although α4–VCAM-1 interactions did not contribute to T cell diapedesis across brain endothelium, endothelial ICAM-1 and ICAM-2 were essentially required for T cell diapedesis across brain endothelium under static conditions (13–16). In this study, we modeled the BBB using pMBMECs that maintain barrier characteristics and the adhesion molecule expression profile of BBB endothelium in an in vitro setting (9, 17, 24). Using wt pMBMECs in static adhesion and diapedesis experimental set-ups similar to our previous studies, we showed a >2-fold increase in T cell adhesion and diapedesis when the pMBMECs were stimulated with TNF-α compared with unstimulated pMBMECs. In line with our previous studies, we confirmed the essential role of endothelial ICAM-1 and ICAM-2 for T cell adhesion to and diapedesis across unstimulated and stimulated pMBMECs under static conditions.

It has now been recognized that investigation of T cell interactions with the endothelium requires live cell imaging tools to detect postarrest T cell dynamics on the endothelium, such as T cell polarization and crawling on the endothelium to permissive sites of diapedesis (5, 25). Moreover, accumulating data show the essential stimulation and, thereby, strengthening of adhesive contacts between T cell-expressed integrins and their respective endothelial ligands by shear forces physiologically exerted by the blood flow (23). To elucidate these recent findings in more detail, we performed live cell-imaging experiments under shear to delineate the individual contributions of endothelial VCAM-1, ICAM-1, and ICAM-2 to the distinct steps of T cell extravasation across the inflamed BBB in vitro.

For all experiments, we used a murine PLP-specific $CD4^+$ Th1 effector/memory T cell line that has been well characterized for its high predisposition to interact with the BBB; in vivo, these T cells migrate across the BBB and induce experimental autoimmune encephalomyelitis (EAE) when injected into susceptible mouse strains (12, 13, 26). As described in this study, these specific highly active T cells are able to interact with the extracellular domain of purified mouse ICAM-1, ICAM-2, or VCAM-1 without coadsorbing any chemokine. This behavior stands in apparent contrast to in vitro studies on the interaction of human T cells with immobilized ICAM-1. These studies were most often executed using freshly prepared peripheral blood T cells representing a heterogeneous population of $CD4^+$ and $CD8^+$ T cells (5, 6, 27). Obviously, human peripheral blood T cells require the presence of a chemokine coimmobilized with ICAM-1 for efficient adhesion and crawling. Whether this apparent difference in T cell behavior is a consequence of different T cell activation status or an intrinsic characteristic of the T cell subtype used remains to be elucidated.

By a thorough comparison of the dynamic interactions of encephalitogenic T cells with wt BBB endothelium and I1-KO, I2-KO, or I1/I2-KO BBB endothelium, we demonstrated that endothelial ICAM-1, but not ICAM-2, mediates shear-resistant T cell arrest on the BBB in vitro. Endothelial VCAM-1 serves as an alternative ligand for T cell arrest on the inflamed BBB endothelium; blocking of VCAM-1 on wt pMBMECs reduced T cell arrest slightly, whereas blocking of VCAM-1 in the absence of ICAM-1 on I1-KO or I1/I2-KO pMBMECs completely abrogated T cell arrest. The specific roles of ICAM-1 and VCAM-1 in mediating T cell arrest were further substantiated by analyzing T cell arrest on immobilized purified ICAM-1, ICAM-2, and VCAM-1.

An important role for VCAM-1 in T cell arrest on the inflamed BBB in vivo was suggested by a number of previous studies. We recently demonstrated that T cells depend on β1-integrins to firmly arrest within the inflamed spinal cord microvasculature during EAE and, therefore, β1-integrin–deficient T cells fail to invade the CNS (28). Similarly, the therapeutic success of the anti–α4-integrin Ab natalizumab in the treatment of MS relies on the inhibition of α4-integrin–mediated arrest of human T cells on the

inflamed BBB in vivo (29, 30). Our present study demonstrates an additional significant involvement of endothelial ICAM-1 in mediating T cell arrest on the inflamed BBB, which suggests that efficient inhibition of T cell arrest on the inflamed BBB in vivo requires blocking of α4β1-integrin–VCAM-1 and LFA-1–ICAM-1 interactions. This might explain the finding that, unlike in other animal models of EAE, blocking α4-integrins was not sufficient to inhibit actively induced EAE in the C57BL/6 mouse (31). Indeed, only the simultaneous blockade of LFA-1 and α4-integrins, but not blocking of either integrin alone, led to instantaneous detachment of encephalitogenic T cells from the vascular walls of meningeal CNS vessels during EAE (2).

Subsequent to shear-resistant T cell arrest, we observed rapid polarization of T cells and their crawling preferentially against the direction of flow on the inflamed BBB. Therefore, our in vitro observations exactly mimic T cell interactions observed in meningeal blood vessels in vivo during EAE: encephalitogenic T cells were observed to crawl against the direction of blood flow to sites permissive for diapedesis (2). In our present study, we determined that ICAM-1 and ICAM-2, but not VCAM-1, mediate T cell polarization and crawling on the endothelium. The role of endothelial ICAM-2 in supporting T cell polarization and crawling became obvious only in the absence of endothelial ICAM-1 on pMBMECs or when studying T cell crawling on immobilized purified ICAM-2. The absence of both ICAMs was required to completely abrogate T cell polarization and crawling on the BBB in vitro. The failure of VCAM-1 to mediate T cell polarization and crawling was confirmed by studying T cell interactions with immobilized purified VCAM-1. T cells seemed to continuously repeat the arrest phase, failed to establish high-avidity interactions, and, therefore, were observed to be pushed along the direction of flow. These findings are in line with our recent studies demonstrating that α4β1-integrins mediate T cell arrest on inflamed BBB microvessels in vivo during EAE (28, 29).

Interestingly, ICAM-1, but not ICAM-2, mediated directed T cell crawling on the BBB endothelium against the direction of flow. Because T cells were able to crawl against the direction of flow on immobilized purified ICAM-2, we speculate that this ability of endothelial ICAM-2 is masked within the physiological context of the endothelial cell surface membrane, probably because of its shorter length compared with ICAM-1 or VCAM-1. Alternatively, the unique ability of endothelial ICAM-1 to support directed T cell crawling against shear on pMBMECs could be explained by a lower molecular density of ICAM-2 compared with ICAM-1 on the surface of the inflamed BBB. Although we showed that the levels of ICAM-1 and ICAM-2 are similar in equally processed IF images, a precise analysis of molecular density remains to be executed.

Recently, clustering of endothelial ICAM-1 beneath the crawling T cell was described in in vitro studies performed under flow conditions (5). Flow conditions exert shear forces on the attached T cell, as well as on endothelial ICAM-1 and ICAM-2 bound to their ligand LFA-1. LFA-1 exists in low-, intermediate-, and high-affinity forms on the T cell surface; it is tightly regulated in its spatial distribution, with intermediate LFA-1 at the leading edge and high-affinity LFA-1 at the mid-zone or on adhesive filopodia capable of invading the endothelial cell (5, 6). Therefore, a differential spatial distribution of endothelial ICAMs on the BBB during their interaction with the T cell could provide an explanation for the different capacities of ICAM-1 and ICAM-2 to support directed crawling. Several recent studies on T cell interaction with HUVECs described enrichment of endothelial ICAM-1, but not of ICAM-2, around T cells in the process of diapedesis, irrespective of whether their route was transcellular or paracellular (25, 32–34). Because ICAM-1 and ICAM-2 represent the main endothelial ligands for T cell crawling, they must be able to withstand traction forces exerted by the crawling motions of the T cell; therefore, a tight anchorage of ICAM-1 and ICAM-2 to the endothelial cytoskeleton would be reasonable. This assumption is supported by our observation that T cells crawl efficiently against the direction of flow on immobilized purified ICAM-1 and ICAM-2 that are laterally fixed and, in consequence, cannot be clustered. Therefore, mechano-sensing of the direction of flow is an intrinsic characteristic of the T cells, and it might be transduced by different signaling molecules intracellularly associated with the individual affinity conformations of LFA-1 (reviewed in Ref. 35).

In summary, our data demonstrate a continuous role for endothelial ICAM-1 in mediating shear-resistant T cell arrest, polarization, and directed crawling on the BBB, whereas VCAM-1 supports T cell arrest but is not involved in the other steps of T cell extravasation. In the absence of endothelial ICAM-1, T cell polarization and crawling on the BBB are mediated by ICAM-2. Thus, blocking a single endothelial adhesion molecule is not sufficient to completely inhibit T cell recruitment into the CNS.

Acknowledgments

We thank Mark Liebi for technical assistance.

Disclosures

The authors have no financial conflicts of interest.

References

1. Ley, K., C. Laudanna, M. I. Cybulsky, and S. Nourshargh. 2007. Getting to the site of inflammation: the leukocyte adhesion cascade updated. *Nat. Rev. Immunol.* 7: 678–689.
2. Bartholomaus, I., N. Kawakami, F. Odoardi, C. Schlager, D. Miljkovic, J. W. Ellwart, W. E. Klinkert, C. Flugel-Koch, T. B. Issekutz, H. Wekerle, and A. Flugel. 2009. Effector T cell interactions with meningeal vascular structures in nascent autoimmune CNS lesions. *Nature* 462: 94–98.
3. Phillipson, M., B. Heit, S. A. Parsons, B. Petri, S. C. Mullaly, P. Colarusso, R. M. Gower, G. Neely, S. I. Simon, and P. Kubes. 2009. Vav1 is essential for mechanotactic crawling and migration of neutrophils out of the inflamed microvasculature. *J. Immunol.* 182: 6870–6878.
4. Luster, A. D., R. Alon, and U. H. von Andrian. 2005. Immune cell migration in inflammation: present and future therapeutic targets. *Nat. Immunol.* 6: 1182–1190.
5. Shulman, Z., V. Shinder, E. Klein, V. Grabovsky, O. Yeger, E. Geron, A. Montresor, M. Bolomini-Vittori, S. W. Feigelson, T. Kirchhausen, et al. 2009. Lymphocyte crawling and transendothelial migration require chemokine triggering of high-affinity LFA-1 integrin. *Immunity* 30: 384–396.
6. Stanley, P., A. Smith, A. McDowall, A. Nicol, D. Zicha, and N. Hogg. 2008. Intermediate-affinity LFA-1 binds alpha-actinin-1 to control migration at the leading edge of the T cell. *EMBO J.* 27: 62–75.
7. Abbott, N. J., A. A. Patabendige, D. E. Dolman, S. R. Yusof, and D. J. Begley. 2010. Structure and function of the blood-brain barrier. *Neurobiol. Dis.* 37: 13–25.
8. Wolburg, H., and A. Lippoldt. 2002. Tight junctions of the blood-brain barrier: development, composition and regulation. *Vascul. Pharmacol.* 38: 323–337.
9. Lyck, R., N. Ruderisch, A. G. Moll, O. Steiner, C. D. Cohen, B. Engelhardt, V. Makrides, and F. Verrey. 2009. Culture-induced changes in blood-brain barrier transcriptome: implications for amino-acid transporters in vivo. *J. Cereb. Blood Flow Metab.* 29: 1491–1502.
10. Wekerle, H., B. Engelhardt, W. Risau, and R. Meyermann. 1990. Passage of lymphocytes across the blood-brain barrier in health and disease. In *In Pathophysiology of the Blood-Brain Barrier.* B. B. Johansson, C. Owman, and H. Widner, eds. Elsevier p. 439–445.
11. Engelhardt, B. 2008. Immune cell entry into the central nervous system: involvement of adhesion molecules and chemokines. *J. Neurol. Sci.* 274: 23–26.
12. Vajkoczy, P., M. Laschinger, and B. Engelhardt. 2001. Alpha4-integrin-VCAM-1 binding mediates G protein-independent capture of encephalitogenic T cell blasts to CNS white matter microvessels. *J. Clin. Invest.* 108: 557–565.
13. Laschinger, M., and B. Engelhardt. 2000. Interaction of alpha4-integrin with VCAM-1 is involved in adhesion of encephalitogenic T cell blasts to brain endothelium but not in their transendothelial migration in vitro. *J. Neuroimmunol.* 102: 32–43.
14. Reiss, Y., and B. Engelhardt. 1999. T cell interaction with ICAM-1-deficient endothelium in vitro: transendothelial migration of different T cell populations is mediated by endothelial ICAM-1 and ICAM-2. *Int. Immunol.* 11: 1527–1539.
15. Lyck, R., Y. Reiss, N. Gerwin, J. Greenwood, P. Adamson, and B. Engelhardt. 2003. T-cell interaction with ICAM-1/ICAM-2 double-deficient brain

endothelium in vitro: the cytoplasmic tail of endothelial ICAM-1 is necessary for transendothelial migration of T cells. *Blood* 102: 3675–3683.
16. Reiss, Y., G. Hoch, U. Deutsch, and B. Engelhardt. 1998. T cell interaction with ICAM-1-deficient endothelium in vitro: essential role for ICAM-1 and ICAM-2 in transendothelial migration of T cells. *Eur. J. Immunol.* 28: 3086–3099.
17. Coisne, C., L. Dehouck, C. Faveeuw, Y. Delplace, F. Miller, C. Landry, C. Morissette, L. Fenart, R. Cecchelli, P. Tremblay, and B. Dehouck. 2005. Mouse syngenic in vitro blood-brain barrier model: a new tool to examine inflammatory events in cerebral endothelium. *Lab. Invest.* 85: 734–746.
18. Gerwin, N., J. A. Gonzalo, C. Lloyd, A. J. Coyle, Y. Reiss, N. Banu, B. Wang, H. Xu, H. Avraham, B. Engelhardt, et al. 1999. Prolonged eosinophil accumulation in allergic lung interstitium of ICAM-2 deficient mice results in extended hyperresponsiveness. *Immunity* 10: 9–19.
19. Xu, H., J. A. Gonzalo, Y. St Pierre, I. R. Williams, T. S. Kupper, R. S. Cotran, T. A. Springer, and J. C. Gutierrez-Ramos. 1994. Leukocytosis and resistance to septic shock in intercellular adhesion molecule 1-deficient mice. *J. Exp. Med.* 180: 95–109.
20. Röhnelt, R. K., G. Hoch, Y. Reiss, and B. Engelhardt. 1997. Immunosurveillance modelled in vitro: naive and memory T cells spontaneously migrate across unstimulated microvascular endothelium. *Int. Immunol.* 9: 435–450.
21. Stein, J. V., S. F. Soriano, C. M'rini, C. Nombela-Arrieta, G. G. de Buitrago, J. M. Rodríguez-Frade, M. Mellado, J. P. Girard, and C. Martínez-A. 2003. CCR7-mediated physiological lymphocyte homing involves activation of a tyrosine kinase pathway. *Blood* 101: 38–44.
22. Lawrence, M. B., C. W. Smith, S. G. Eskin, and L. V. McIntire. 1990. Effect of venous shear stress on CD18-mediated neutrophil adhesion to cultured endothelium. *Blood* 75: 227–237.
23. Alon, R., and M. L. Dustin. 2007. Force as a facilitator of integrin conformational changes during leukocyte arrest on blood vessels and antigen-presenting cells. *Immunity* 26: 17–27.
24. Coisne, C., C. Faveeuw, Y. Delplace, L. Dehouck, F. Miller, R. Cecchelli, and B. Dehouck. 2006. Differential expression of selectins by mouse brain capillary endothelial cells in vitro in response to distinct inflammatory stimuli. *Neurosci. Lett.* 392: 216–220.
25. Carman, C. V., P. T. Sage, T. E. Sciuto, M. A. de la Fuente, R. S. Geha, H. D. Ochs, H. F. Dvorak, A. M. Dvorak, and T. A. Springer. 2007. Transcellular diapedesis is initiated by invasive podosomes. *Immunity* 26: 784–797.
26. Engelhardt, B., M. Laschinger, M. Schulz, U. Samulowitz, D. Vestweber, and G. Hoch. 1998. The development of experimental autoimmune encephalomyelitis in the mouse requires alpha4-integrin but not alpha4beta7-integrin. *J. Clin. Invest.* 102: 2096–2105.
27. Takesono, A., S. J. Heasman, B. Wojciak-Stothard, R. Garg, and A. J. Ridley. 2010. Microtubules regulate migratory polarity through Rho/ROCK signaling in T cells. *PLoS ONE* 5: e8774.
28. Bauer, M., C. Brakebusch, C. Coisne, M. Sixt, H. Wekerle, B. Engelhardt, and R. Fässler. 2009. Beta1 integrins differentially control extravasation of inflammatory cell subsets into the CNS during autoimmunity. *Proc. Natl. Acad. Sci. USA* 106: 1920–1925.
29. Coisne, C., W. Mao, and B. Engelhardt. 2009. Cutting edge: Natalizumab blocks adhesion but not initial contact of human T cells to the blood-brain barrier in vivo in an animal model of multiple sclerosis. *J. Immunol.* 182: 5909–5913.
30. Engelhardt, B., and L. Kappos. 2008. Natalizumab: targeting alpha4-integrins in multiple sclerosis. *Neurodegener. Dis.* 5: 16–22.
31. Kerfoot, S. M., M. U. Norman, B. M. Lapointe, C. S. Bonder, L. Zbytnuik, and P. Kubes. 2006. Reevaluation of P-selectin and alpha 4 integrin as targets for the treatment of experimental autoimmune encephalomyelitis. *J. Immunol.* 176: 6225–6234.
32. Millán, J., L. Hewlett, M. Glyn, D. Toomre, P. Clark, and A. J. Ridley. 2006. Lymphocyte transcellular migration occurs through recruitment of endothelial ICAM-1 to caveola- and F-actin-rich domains. *Nat. Cell Biol.* 8: 113–123.
33. Carman, C. V., and T. A. Springer. 2004. A transmigratory cup in leukocyte diapedesis both through individual vascular endothelial cells and between them. *J. Cell Biol.* 167: 377–388.
34. Barreiro, O., M. Yanez-Mo, J. M. Serrador, M. C. Montoya, M. Vicente-Manzanares, R. Tejedor, H. Furthmayr, and F. Sanchez-Madrid. 2002. Dynamic interaction of VCAM-1 and ICAM-1 with moesin and ezrin in a novel endothelial docking structure for adherent leukocytes. *J. Cell Biol.* 157: 1233–1245.
35. Smith, A., P. Stanley, K. Jones, L. Svensson, A. McDowall, and N. Hogg. 2007. The role of the integrin LFA-1 in T-lymphocyte migration. *Immunol. Rev.* 218: 135–146.
36. Cecchelli, R., B. Dehouck, L. Descamps, L. Fenart, V. V. Buée-Scherrer, V, C. Duhem, S. Lundquist, M. Rentfel, G. Torpier, and M. P. Dehouck. 1999. In vitro model for evaluating drug transport across the blood-brain barrier. *Adv. Drug Deliv. Rev.* 36: 165–178.